NANO LETTERS

Letter

Photon-Assisted Tunneling in a Carbon Nanotube Quantum Dot

Carola Meyer, Jeroen M. Elzerman, and Leo P. Kouwenhoven

Nano Lett., **2007**, 7 (2), 295-299 • DOI: 10.1021/nl062273j

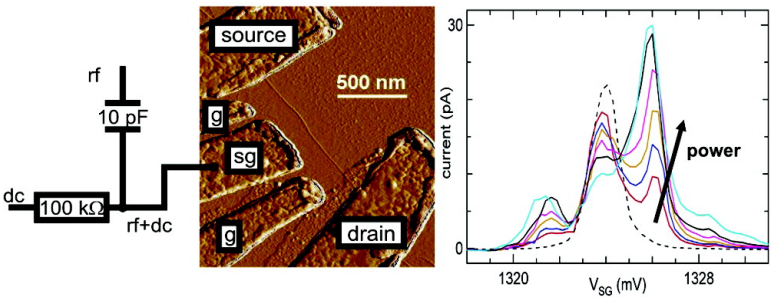

More About This Article

Additional resources and features associated with this article are available within the HTML version:

- Supporting Information
- Links to the 3 articles that cite this article, as of the time of this article download
- Access to high resolution figures
- Links to articles and content related to this article
- Copyright permission to reproduce figures and/or text from this article

View the Full Text HTML

Nano Letters is published by the American Chemical Society. 1155 Sixteenth Street N.W., Washington, DC 20036

NANO LETTERS

2007
Vol. 7, No. 2
295−299

Photon-Assisted Tunneling in a Carbon Nanotube Quantum Dot

Carola Meyer,*,†,‡ Jeroen M. Elzerman,‡,§ and Leo P. Kouwenhoven‡

Research Centre Jülich, Institute of Solid State Research, Electronic Properties, 52425 Jülich, Germany, Kavli Institute of Nanoscience, Delft University of Technology, P.O. Box 5046, 2600 GA Delft, The Netherlands, and Institute of Quantum Electronics, ETH Zürich, CH-8093 Zürich, Switzerland

Received September 27, 2006; Revised Manuscript Received December 22, 2006

ABSTRACT

We report on photon-assisted tunneling (PAT) experiments in a carbon nanotube quantum dot using microwave frequencies between 20 and 60 GHz. In addition to the basic PAT effect, revealed by the appearance of two extra resonances in the current through the dot, we use PAT for spectroscopy of excited states. The experimental data are in good agreement with simulations.

High-frequency transport properties of carbon nanotube devices have received a lot of interest in connection with, e.g., the performance of radio frequency field effect transistors (rf-FETs)[1,2] and nano electromechanical systems.[3] Most of the experiments have been carried out at frequencies below 1 GHz. Only very recently, frequencies of 10 GHz and more have been used in ac transport[4] and with rf-FETs.[5] All these studies have been done at room temperature. However, the response of a carbon nanotube in the low-temperature quantum transport regime is very interesting for future devices such as radio frequency single electron transistors (rf-SETs)[6−8] or quantum dots used for information processing (QIP).[9]

Control over a charge[10] or spin[11,12] qubit using high-frequency pulses has already been demonstrated for GaAs quantum dots. However, electron spins in carbon nanotubes (CNTs) are expected to have longer relaxation times due to the small spin-orbit coupling and the possible absence of nuclear spins, which are known to be the dominant spin relaxation mechanisms in GaAs.[13−15] This could make CNT quantum dots very suitable candidates for a solid-state qubit system. We study photon-assisted tunneling (PAT) in a CNT quantum dot as a first step toward high-frequency control over such a spin qubit.

In this Letter we present a device structure for PAT experiments on CNT quantum dots. We show the direct PAT process and use photon-assisted tunneling to perform spectroscopy on excited states. Furthermore, we compare data of power-dependent measurements to the simulation of a model system.

* Corresponding author: c.meyer@fz-juelich.de.
† Research Centre Jülich, Institute of Solid State Research.
‡ Kavli Institute of Nanoscience, Delft University of Technology.
§ Institute of Quantum Electronics, ETH Zürich.

10.1021/nl062273j CCC: $37.00
Published on Web 01/18/2007

Single-walled carbon nanotubes (SWCNTs) are grown using chemical vapor deposition (CVD)[16] on a patterned Si/SiO_2 substrate. In contrast to the field effect transistor structures most often used for quantum transport in CNTs, we do not use highly doped Si to avoid leakage of the high-frequency signal to the back gate. The quantum dot is formed between aluminum source/drain contacts, and the potential can be tuned using an aluminum side-gate (see Figure 1). The low work function of aluminum ensures high tunnel barriers at low temperatures.[17] The tube diameter in the device used for the presented measurements is only $d \sim 1$ nm, which implies a higher contact resistance compared to larger diameters.[18] In order to get a resistance smaller than 1 GΩ, we evaporated 1 nm of Ti before evaporating the aluminum. This way, we achieved tunnel rates $\Gamma \ll h\nu$, with ν the frequency of the rf signal, which allows us to clearly resolve the microwave-induced side peaks.[19]

All measurements are performed at the base temperature of a dilution refrigerator. The high-frequency signal and dc gate voltage are added with a bias-tee at base temperature (∼25 mK) and applied to the side gate. Two guard electrodes surrounding it are set to ground and suppress the capacitive coupling of the side gate to source and drain contacts. To transport the microwave signal to the device, we use semirigid coaxial lines thermally anchored at 4 K, 1 K, ∼700 mK, and base temperature. The inner conductor is cooled with −3 dB attenuators at 1 K and at ∼700 mK, plus a −10 dB attenuator at base temperature (except where noted otherwise).

Under microwave irradiation of the nanotube quantum dot, we expect photon-assisted tunneling to be revealed by the appearance of two current side peaks.[20] The splitting of these peaks should depend linearly on frequency.[19,21] The ampli-

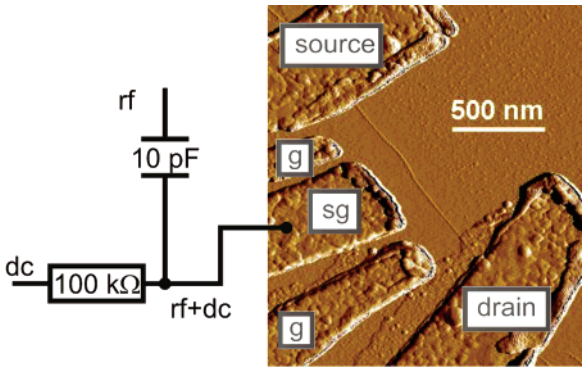

Figure 1. Schematic layout of the device with low-temperature bias-tee and atomic force microscopy (AFM) picture of a similar device as the one used for the experiments discussed here. The actual device (not shown here) has a total nanotube length of 940 nm between the Al contacts. The side gate (sg), which is flanked by two guard electrodes (g), has a width of 410 nm, and its distance to the CNT is about 200 nm. The height of the tube measured with AFM in tapping mode is 1 nm. Room temperature measurements of the quasi-metallic tube show a resistance of 48 kΩ.

tudes of the main Coulomb resonance and the side peaks should depend on the amplitude V of the applied signal $V_{ac} = V\cos(2\pi\nu t)$ and follow the Bessel function $J_n^2(\alpha)$, with $\alpha = eV/h\nu$ and n the number of photons of energy $h\nu$ (with $n = 0$ for the main Coulomb resonance).[19]

Figure 2 shows measurements of current versus gate voltage of the unperturbed Coulomb peak (dashed curve) and the peak splitting under high-frequency irradiation. Frequencies are chosen such that the signal shows only small interference with electron pumping, which occurs if the rf signal couples differently to source and drain tunnel barriers.[19,22] As expected, the total splitting between the extra resonances in the current is $2h\nu$ and increases linearly with frequency.

The insets of Figure 2 describe the PAT processes of a single-level system for the left and right side peak, respectively. Left of the main Coulomb resonance, when the quantum dot is in its N electron state and the electrochemical potential of the $N \leftrightarrow N + 1$ resonance is above the bias window, an electron in the left lead can absorb a photon and tunnel onto the dot. This electron can then leave the dot to both sides with the same probability, but it contributes to the current only if it tunnels to the right lead. This process is frequency dependent, because as soon as an electron from the right lead can also absorb a photon and tunnel onto the dot, the net current from these two processes will be zero. To the right of the main resonance, where the quantum dot is in its $N + 1$ stable state, an electron on the dot can absorb a photon and tunnel out to the right lead. An electron can then enter from the Fermi sea of either of the leads and refill the level, but it contributes to the current only when entering from the left. If the photon energy is large enough so that the electron can tunnel to both leads, again there is no net current.

The amplitude of the PAT peaks observed is smaller at higher frequencies. This is due to reflection of the rf signal at the SMA connector used to couple the coaxial lines to the chip carrier.[24] This also explains why two-photon

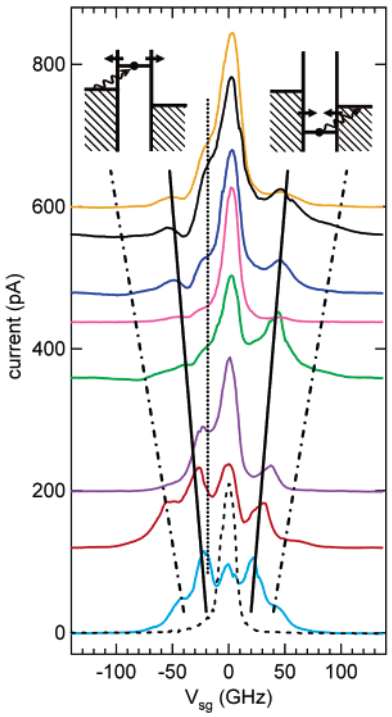

Figure 2. Photon-assisted tunneling at different frequencies: ac source voltage amplitude $V_{ac} = 71$ mV (−10 dBm), bias voltage $V_{SD} = 50$ μeV. The dc side gate voltage V_{SG} is swept from 266.4 to 300 mV and converted to an energy shift in GHz, using a conversion factor for the gate voltage to energy of $C_g/C_\Sigma \sim 0.03$ (obtained from stability diagrams at 4 K). The Coulomb peak measured without rf irradiation (dashed curve) is compared to the traces at 20, 26, 30, 38, 42, 44, 48, and 50 GHz (from bottom to top). The curves are offset in proportion to the frequency. The insets describe the basic PAT process below (left inset) and above (right inset) the main resonance. The black straight lines are guides to the eye for the one-photon satellites (solid) at positions $\pm h\nu$ away from the main Coulomb resonance, the two-photon side peaks (dash-dotted), and a frequency independent excited state that is visible at higher frequencies (dotted). The electron temperature in this measurement was around 210 mK, higher than any in the rest of the paper, due to the absence of the microwave attenuator at base temperature.

processes with splitting $4h\nu$ are apparent only for frequencies below 30 GHz. A shoulder that does not move with frequency is visible at $\delta\epsilon \sim 70$ μeV and can be clearly distinguished from the PAT peaks only above $\nu = 30$ GHz, i.e., for $h\nu > 1.5\delta\epsilon$. As will be discussed below, this corresponds to transport via an excited state.

In order to investigate these features more closely, we installed a −10 dB attenuator at the mixing chamber, reducing the electron temperature to below 170 mK. We then performed excited-state spectroscopy with PAT, as shown in Figure 3. In contrast to the measurements shown in Figure 2, the peaks to the left and right of the main resonance in Figure 3a are neither split by the amount expected for direct PAT induced peaks nor move with microwave frequency. Instead, they have their origin in tunneling through excited states initiated by a PAT process. The peaks of the direct PAT process are not visible due to the small microwave power. This becomes apparent in the power dependence of the peaks investigated at $\nu = 40.8$ GHz, as shown in Figure 3b. Direct PAT processes such as those shown in Figure 2

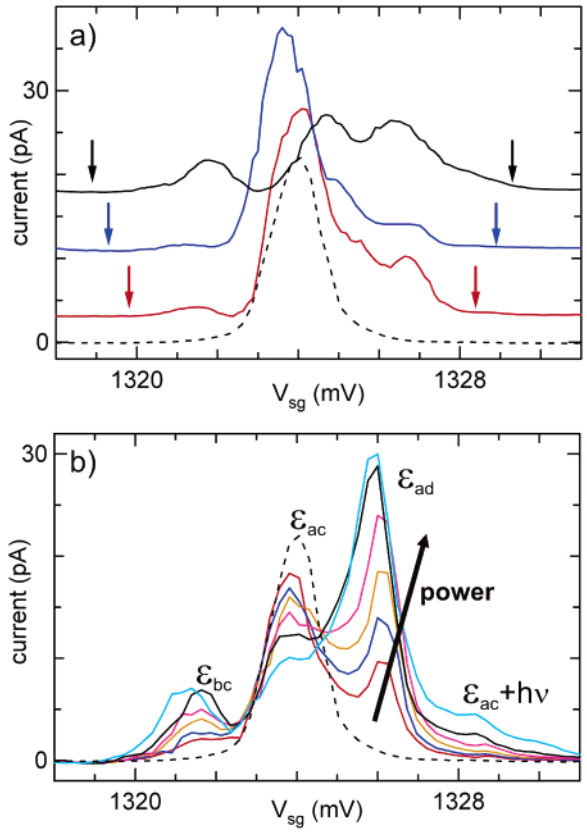

Figure 3. Excited-state spectroscopy using PAT as a function of dc side-gate voltage V_{SG}, with bias $V_{SD} = 50\ \mu$eV. (a) Different frequencies at fixed rf source amplitude $V_{ac} = 56$ mV (the lines are offset for clarity). Arrows mark the positions where PAT peaks are expected for 36.31 GHz (red), 40.51 GHz (blue), and 43.91 GHz (black solid line), with $C_g/C_\Sigma \sim 0.035$. The highest frequency shows some asymmetry on the central peak due to pumping. Nevertheless, it is clear that the two lines to the left and right of the Coulomb peak do not show the right frequency-dependent splitting for PAT satellites but have their origin in excited states. (b) Power dependence ($V_{ac} = 89-282$ mV) of the peaks at 40.8 GHz, where pumping effects are small.

are observed at higher microwave amplitudes, but only for $\epsilon_{ac} + h\nu$. The peak at $\epsilon_{ac} - h\nu$ is suppressed due to overlap of a small, nearly power independent, pumping signal.[25]

The peaks attributed to transport through excited states are more apparent at high power while the main resonance, ϵ_{ac}, decreases. Similar behavior has been observed in GaAs dots.[25,26] We emphasize, however, that the PAT-induced excited-state peak denoted here as ϵ_{bc} has not been reported before, to the best of our knowledge. The excited-state peaks occur at positions $\delta\epsilon_{bc} = -83(7)\ \mu$eV and $\delta\epsilon_{ad} = 70(7)\ \mu$eV relative to the Coulomb peak.

The levels and rates involved in the process are depicted in Figure 4. The situation can be described as follows (a more detailed figure is given in the Supporting Information): All in all, four levels are involved denoted a, b, c, and d. Levels a and b are the ground and first excited state of the N electron quantum dot. Ground and first excited state of the quantum dot with $N + 1$ electrons are labeled c and d. The electrochemical potential $\mu_{ac}(N + 1) = U_c(N + 1) - U_a(N)$ of the quantum dot, with $U_a(N)$ the ground-state energy of the N electron QD and $U_c(N + 1)$ the ground-state energy

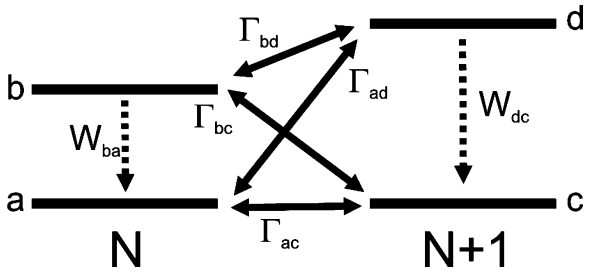

Figure 4. Schematic drawing of the levels and rates involved in PAT spectroscopy: During transport the number of electrons fluctuates between N and $N + 1$. Ground-state tunneling between states a and c corresponds to the peak ϵ_{ac}, while tunneling between the N-electron excited state b and $N + 1$ ground state c (between N-electron ground state a and $N + 1$ excited state d) corresponds to peak ϵ_{bc} (ϵ_{ad}). The tunneling rates Γ and relaxation rates W between related states are named accordingly.

of the $N + 1$ electron QD, respectively, has to be aligned within the bias window, in order to get transport via ground-state tunneling between N and $N + 1$ electrons. Transport via excited states can occur if the corresponding ground state is not occupied and the electrochemical potential $\mu_{ad}(N + 1)$ (or $\mu_{bc}(N + 1)$) is aligned within the bias window.

At the ϵ_{ad} peak, tunneling with tunneling rate Γ_{ad} occurs between the N electron ground state and an $N + 1$ excited state at $\mu_{ad}(N + 1) = U_d(N + 1) - U_a(N) > \mu_{ac}(N + 1)$ and therefore at higher electrochemical potential than the main Coulomb resonance. The energy difference to the main resonance is $\delta\epsilon_{ad}(N + 1) = \mu_{ad}(N + 1) - \mu_{ac}(N + 1) = U_d(N + 1) - U_c(N + 1) = 70(7)\ \mu$eV (compare Figure 3).

In the case of the ϵ_{bc} peak, tunneling occurs between an N-electron excited state and the $N + 1$ ground state. The corresponding resonance has a lower electrochemical potential than the main Coulomb resonance, because $\mu_{bc}(N + 1) = U_c(N + 1) - U_b(N) < \mu_{ac}(N + 1)$. The distance to the main resonance is $\delta\epsilon_{bc}(N) = \mu_{bc}(N + 1) - \mu_{ac}(N + 1) = -U_b(N) + U_a(N) = -83(7)\ \mu$eV. Such a PAT peak (involving an N-electron excited state) has, to our knowledge, never been reported in PAT experiments on GaAs single quantum dots.

For better understanding of the power dependence of the excited states, we compare our data to the simulation of a model system. In the following, we describe the model and give the equations used for the simulation before showing the results.

In a photon-assisted tunneling (PAT) experiment, an ac voltage drop $V_{ac} = V\cos(2\pi\nu t)$ over a tunnel barrier modifies the tunnel rate $\Gamma_{PAT}(E) = \sum_n J_n^2(\alpha)\,\Gamma\,(E + nh\nu)$[19] analogous to the theory for a junction between two superconducting leads.[27] $J_n^2(\alpha)$ is the nth order Bessel function of the first kind with $\alpha = eV/h\nu$. Γ_{PAT} and Γ are the tunneling rates with and without microwave irradiation.

We use a model[28] with four states as in Figure 4, because in our device the charging energy E_C is much larger than all other energies involved $E_C \gg h\nu, \delta\epsilon, k_BT, V_{SD}$. If we neglect level broadening and relaxation, the current through the quantum dot in a certain configuration χ (χ = a,b,c,d) can be described by the probability P_χ that the dot is in a

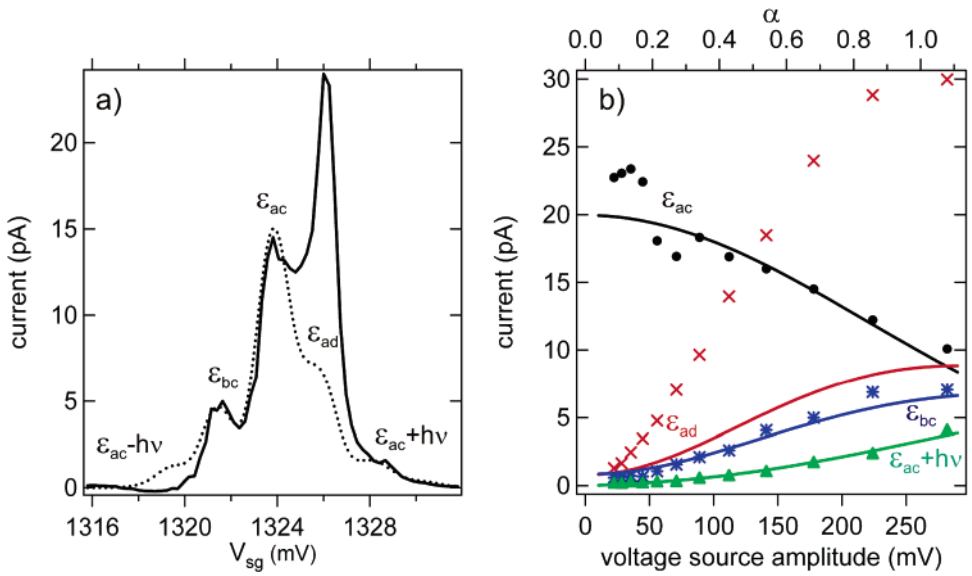

Figure 5. (a) Comparison between measured current (solid line) at voltage source amplitude $V_{ac} = 178$ mV and simulated current (dotted) at $\alpha = 0.635$ and $\nu = 40.8$ GHz. (b) Comparison of simulated current at the different peak positions (solid lines) with data (symbols). Comparing the factor α of the simulation with the rf source amplitude, the overall attenuation of the system is found to be −63.4 dB. Attenuators put in the lines add up to −33 dB. Thus, the coaxial lines and reflection at the connection to the sample reduce the signal by additional 30.4 dB for this frequency.

particular configuration, together with the tunnel rates through a single barrier[29]

$$I = e[P_a(\Gamma^{in}_{l,ac} + \Gamma^{in}_{l,ad}) + P_b(\Gamma^{in}_{l,bc} + \Gamma^{in}_{l,bd}) - P_c(\Gamma^{out}_{l,ac} + \Gamma^{out}_{l,bd}) - P_d(\Gamma^{out}_{l,ad} + \Gamma^{out}_{l,bd})] \quad (1)$$

Here, $\Gamma^{in(out)}_{l,j}$ is the tunnel rate into (out of) the dot via transition j, through the left barrier

$$\Gamma^{in}_{l/r,j}(\epsilon_j) = \Gamma_{l/r,j} \sum_n J_n^2(eV/h\nu) f(\epsilon_j - (C_g/C)eV_g - nh\nu - 0.5V_{SD}; k_BT)$$

$$\Gamma^{out}_{l/r,j}(\epsilon_j) = \Gamma_{l/r,j} \sum_n J_n^2(eV/h\nu)[1 - f(\epsilon_j - (C_g/C)eV_g - nh\nu - 0.5V_{SD}; k_BT)] \quad (2)$$

with ϵ_j the electrochemical potential of transition j (with $j =$ ac, ad, bc, bd), $f(E;k_BT)$ the Fermi function at temperature T, V_g the gate voltage, C_g the gate capacitance, $C = C_1 + C_2 + C_g$ with $C_{1(2)}$ the capacitance of the left(right) barrier, and source−drain voltage V_{SD}. The factor 0.5 is used to describe an equal voltage drop over the left and right barrier. The factor $\alpha = eV/h\nu$ gives the coupling of the microwaves to the barriers.

In order to find the occupation probabilities P_χ, we calculate the stationary solution of the rate equations for the four-level system (see Supporting Information), using eqs 2. The results are inserted in (1) to calculate the current for different microwave-coupling coefficients, α. The source-drain voltage is taken as in the experiment $V_{SD} = 50$ μeV, and tunnel rates Γ_j are obtained from a measurement of Coulomb diamonds, yielding $\Gamma_{ac} = 0.17$ GHz, $\Gamma_{ad} = 0.28$ GHz, and $\Gamma_{bc} = 0.16$ GHz, respectively. (However, this gives only the total tunnel rate and for comparison with the data we assume that the barriers are equal, and therefore $\Gamma_{l/r,j} = 2\Gamma_j$).

In Figure 5, we compare the result of the simulation (solid lines) with the data (dashed lines). Note that we cannot calculate the actual factor α, because of the unknown reflection at the sample holder and at the bonding from the chip carrier to the sample. Thus, α is chosen such that the current is matched best (see Figure 5a as example).

We find good agreement for the main resonance (black), the ϵ_{bc} peak (blue), and the peak of $\epsilon_{ac} + h\nu$ (green) with transition rate between the two excited states $\Gamma_{bd} = 0$, and relaxation rates $W_{ba} = W_{dc} = 0$ while assuming a small asymmetry in the coupling of the microwaves to the barriers ($\alpha_l = 0.95\alpha_r$). The functional dependence of the peak ϵ_{ad} (red) on the microwave power α is the same in the simulation as in the data. However, the current is strongly enhanced compared to the simulation. A similar behavior has been observed for GaAs quantum dots as well and was explained by intradot excitations.[26]

Such a scenario could be responsible for the enhanced peak ϵ_{ad} measured here. We note that peak ϵ_{bc}, on the other hand, is very well reproduced by our model without assuming intradot excitation, which could indicate that the microwaves are not efficiently creating intradot excitations in the N-electron case. A more detailed model is required to verify these assumptions.

Introducing energy relaxation W_{ba}, W_{dc} (compare Figure 4) faster than about a GHz into the simulation changes the curve shapes and shifts the peak slopes with respect to each other in a way that cannot be compensated by adjusting α. Thus, we can say that the model involving four levels

describes the measurements without assuming relaxation (in the order of nanoseconds) for the first excited states b and d.

In conclusion, we have shown photon-assisted tunneling in a carbon nanotube quantum dot. We use aluminum for source and drain electrodes to ensure small tunneling rates at low temperatures. With this setup, we observe the expected peak splitting under high-frequency irradiation, and even two-photon processes are visible. We also observe frequency-independent peaks related to excited states in the quantum dot. Simulations of a four-level model show good agreement with the data, although one of the peaks is strongly enhanced. This has been observed in GaAs quantum dots as well and can be explained by intradot excitation. The second peak related to another excited state has, to the best of our knowledge, not been reported for GaAs.

These observations are the first steps toward high-frequency control of carbon nanotube quantum dots, which is vital for using spin in nanotubes for quantum information processing.

Acknowledgment. We thank R. Schouten for discussions about high-frequency electronics as well as H. Schoeller and W. van der Wiel for discussions about PAT spectroscopy. We also thank C. Dekker for the use of the CNT growth facilities. This work was financially supported by the Defense Advanced Research Projects Agency Quantum Information Science and Technology program, the Dutch Organization for Fundamental Research on Matter (FOM), The Netherlands Organization for Scientific Research (NWO), and the EU Research Training Network on spintronics.

Supporting Information Available: Supporting measurements of Coulomb diamonds that show the excited states studied in PAT spectroscopy, rate equations used for the simulation of the current, and a detailed scheme that depicts the transport through the excited states. This material is available free of charge via the Internet at http://pubs.acs.org.

References

(1) Appenzeller, J.; Frank, D. J. *Appl. Phys. Lett.* **2004**, *84*, 1771.
(2) Staii, C.; Johnsson, A. T., Jr.; Shao, R.; Bonnell, A. *Nano Lett.* **2005**, *5*, 893.
(3) Sazonova, V.; Yaish, Y.; Üstünel, H.; Roundy, D.; Arias, T. A.; McEuen, P. L. *Nature* **2004**, *431*, 284.
(4) Yu, Z.; Burke, P. J. *Nano Lett.* **2005**, *5*, 1403.
(5) Pesetski, A. A.; Baumgardner, J. E.; Folk, E.; Przybysz, J. X.; Adam, J. D.; Zhang, H. *Appl. Phys. Lett.* **2006**, *88*, 113103.
(6) Schoelkopf, R. J.; Wahlgren, P.; Kozhevnikov, A. A.; Delsing, P.; Prober, D. E. *Science* **1998**, *280*, 1238.
(7) Roschier, L.; Sillanpää, M.; Taihong, W.; Ahlskog, M.; Iijima, S.; Hakonen, P. *J. Low Temp. Phys.* **2004**, *136*, 465.
(8) Li, S.; Yu, Z.; Yen, S.-F.; Tang, W. C.; J. Burke, J. *Nano Lett.* **2004**, *4*, 753.
(9) Loss, D.; Vincenzo, D. *Phys. Rev. A* **1998**, *57*, 120.
(10) Hayashi, T.; Fujisawa, T.; Cheaong, H. D.; Jeong, Y. H.; Hirayama, Y. *Phys. Rev. Lett.* **2003**, *91*, 226804.
(11) Petta, J. R.; Johnson, A. C.; Taylor, J. M.; Laird, E. A.; Yacoby, A.; Lukin, M. D.; Marcus, C. M.; Hanson, M. P.; Gossard, A. C. *Science* **2005**, *309*, 2180.
(12) Koppens, F. H. L.; Buizert, C.; Tielrooij, K. J.; Vink, I. T.; Nowack, K. C.; Meunier, T.; Kouwenhoven, L. P.; Vandersypen, L. M. K. *Nature* **2006**, *442*, 766.
(13) Khaetskii, A. V.; Nazarov, Y. V. *Phys. Rev. B* **2000**, *61*, 12639.
(14) Woods, L. M.; Reinecke, T. L.; Lyanda-Geller, Y. *Phys. Rev. B* **2002**, *66*, 161318.
(15) Golovach, V. N.; Khaetskii, A.; Loss, D. *Phys. Rev. Lett.* **2004**, *93*, 016601.
(16) Kong, J.; Soh, H. T.; Cassell, A. M.; Quate, C. F.; Dai, H. *Nature* **1998**, *395*, 878.
(17) Yang, M. H.; Teo, K. B. K.; Milne, W. I.; Hasko, D. G. *Appl. Phys. Lett.* **2005**, *87*, 253116.
(18) Kim, W.; Javey, A.; Tu, R.; Cao, J.; Wang, Q.; Dai, H. *Appl. Phys. Lett.* **2005**, *87*, 173101.
(19) Kouwenhoven, L. P.; Jauhar, S.; McCormick, K.; Dixon, D.; McEuen, P. L.; Nazarov, Yu. V.; van der Vaart, N. C.; Foxon, C. T. *Phys. Rev. B* **1994**, *50*, 2019.
(20) Oosterkamp, T. H.; Kouwenhoven, L. P.; Koolen, A. E. A.; van der Vaart, N. C.; Harmans, C. J. P. M. *Phys. Rev. Lett.* **1997**, *78*, 1536.
(21) Kouwenhoven, L. P.; Jauhar, S.; Orenstein, J.; McEuen, P. L.; Nagamune, Y.; Motohisa, J.; Sakaki, H. *Phys. Rev. Lett.* **1994**, *73*, 3443.
(22) Bruder, C.; Schoeller, H. *Phys. Rev. Lett.* **1994**, *72*, 1076.
(23) Lemay, S. G.; Janssen, J. W.; van den Hout, M.; Mooij, M.; Bronikowski, J. M.; Willis, P. A.; Smalley, R. E.; Kouwenhoven, L. P.; Dekker, C. *Nature* **2001**, *412*, 617.
(24) The SMA standard is specified to transmit signals up to 18 GHz, and usually the reflection up to ∼21 GHz is small. Above that, it gets stronger with frequency. Additionally, we have reflection due to the bonding on the chip and also the stripline designed on the chip is not matched to 50 Ω. Thus, without measuring the power dependence of the signal, we do not know the amplitude of the signal that actually reaches the device.
(25) van der Wiel, W. G.; Oosterkamp, T. H.; De Franceschi, S.; Harmans, C. J. P. M.; Kouwenhoven, L. P. *Proceedings of the NATO Advanced Study Institute on Strongly Correlated Fermions and Bosons in Low-Dimensional Disordered Systems*, Windsor, U.K. 13−26. August 2001; Lerner, I. V., Althsuler, B. L., Fal'ko, V. I., Giamarchi, T., Eds.; Kluwer Academic Publishers: Dordrecht, 2001; pp 43−68. ISBN 1-4020.-0748-5.
(26) Brune, Ph.; Bruder, C.; Schoeller, H. *Phys. Rev. B* **1997**, *56*, 4730.
(27) Tien, P. K.; Gordon, J. R. *Phys. Rev.* **1967**, *129*, 647.
(28) Wan, C. J.; McGreer, K. A.; Glazman, L. I.; Goldman, A. M.; Shekther, R. I. *Phys. Rev. B* **1991**, *43*, 9381.
(29) Oosterkamp, T. H.; Kouwenhoven, L. P.; Koolen, A. E. A.; van der Vaart, N. C.; Harmans, C. J. P. M. *Semicond. Sci. Technol.* **1996**, *11*, 1512.

NL062273J